Chapter 3

CTMQC applied to molecular systems

In order to apply CTMQC to large molecular systems (hundreds of molecules) a different way to construct the Hamiltonian is needed. In this work I have implemented the CTMQC equations within the fragment-orbital based framework. This relies on the equations being expressed in a pseudo-diabatic basis and the Hamiltonian being constructed in 2 parts: the diagonal elements (site energies) and the off-diagonals (electronic couplings). The basis is termed 'pseudo-diabatic' due to the fact that non-adiabatic coupling vectors are small but non vanishing, this results in a basis where the excess charge carrier is strongly but not strictly localised on a single molecule. Within the Hamiltonian, the site energies are calculated via classical force-fields and the electronic couplings are calculated via the analytic overlap method[58,60] (AOM). In this method the coupling elements are assumed to be proportional to the overlap between the highest singly occupied molecular orbitals (SOMO) on the donor and acceptor molecules (see equation (3.1)). This approximation is often used in the literature, e.g. in the fragment orbital density functional theory[65–67] (FODFT) method and has been shown to be valid for π-conjugated molecules[58,68].

$$H_{ab} = C\langle\varphi_a|\varphi_b\rangle = CS_{ab} \tag{3.1}$$

Where $\varphi_{a(b)}$ represents a singly occupied molecular orbital on the donor (acceptor) and C is the scaling constant and comes from DFT parameterisation. The singly occupied molecular orbitals are calculated as a linear combination of Slater-type orbitals (STO) as in equation (3.2). In this equation we loop over each atom in the molecule and sum

the size of the contribution, $c_{p\pi,i}$, multiplied by the STO, $p_{\pi,j}$. In this case the STO is represented by a p-orbital. The size of the p-orbital on each atom, $c_{p\pi,i}$, is parameterised before the simulation with DFT.

$$|\varphi_{mol}\rangle = \sum_{i \in mol}^{N_{\text{atoms}}} c_{p\pi,i} |p_{\pi,i}\rangle \tag{3.2}$$

Importantly, the AOM method offers a very fast way to calculate the off-diagonal elements of the hamiltonian via a finite-difference method with an accuracy comparable to that of DFT methods[69]. This has been implemented within an open-source software package named CP2K and is used by a fragment-orbital based surface hopping technique to study large systems of hundreds of molecules. In the next chapter the surface hopping technique will be discussed in further detail and applied to a system of pentacene molecules in order to investigate charge carrier (hole) transfer within amorphous systems.

3.1 Basis Transformation

In order to use the FOB method, as stated above the CTMQC equations in the adiabatic basis must be transformed to the diabatic basis. In the following derivation C_l will represent the adiabatic expansion coefficient corresponding to state l and u_l will represent the orthogonal diabatic expansion coefficients.

The CTMQC equations in the adiabatic basis are given below in equation (3.3) of the forces and (3.4) coefficients:

$$\begin{aligned} \mathbf{F}_\nu^{(I)} = &- \sum_k |C_k^{(I)}|^2 \nabla_\nu E_k^{(I)} - \sum_{k,l} C_l^{*(I)} C_k^{(I)} \left(E_k^{(I)} - E_l^{(I)} \right) \mathbf{d}_{\nu,lk}^{ad,(I)} \\ &- \sum_{l,k} |C_l^{(I)}|^2 \left(\sum_{\nu'}^{N_n} \frac{2}{\hbar M_{\nu'}} \mathscr{Q}_{\nu',lk}^{(I)} \cdot \mathbf{f}_{l,\nu'}^{(I)} \right) \left[\mathbf{f}_{k,\nu}^{(I)} - \mathbf{f}_{l,\nu}^{(I)} \right] |C_k^{(I)}|^2 \end{aligned} \tag{3.3}$$

$$\begin{aligned}\dot{C}_l^{(I)} = &-\frac{i}{\hbar}E_l^{(I)}C_l^{(I)} - \sum_k C_k^{(I)} \sum_{\nu=1}^{N_n} \frac{\mathbf{P}_\nu^{(I)}}{M_\nu} \cdot \mathbf{d}_{\nu,lk}^{ad,(I)} \\ &- \sum_{\nu=1}^{N_n} \sum_k \frac{\mathscr{Q}_{\nu,lk}^{(I)}}{\hbar M_{\nu'}} \cdot \left[\mathbf{f}_{k,\nu}^{(I)} - \mathbf{f}_{l,\nu}^{(I)}\right] |C_k^{(I)}|^2 C_l^{(I)}\end{aligned} \tag{3.4}$$

Where:

- $E_k^{(I)}$ is the adiabatic energy for state k and trajectory I
- $C_k^{(I)}$ is the adiabatic expansion coefficient for state k and trajectory I
- $\mathbf{P}_\nu^{(I)}$ is the classical momentum of atom ν on trajectory I
- $\mathbf{d}_{\nu,lk}^{ad,(I)}$ is the nonadiabatic coupling vector (given in the adiabatic basis)
- M_ν is the mass of nuclei ν
- $\mathscr{Q}_{\nu,lk}^{(I)}$ is the quantum momentum vector for atom ν corresponding to the lk pair of states in trajectory I
- $\mathbf{f}_{l,\nu}^{(I)}$ is the adiabatic momentum on state l, atom ν and trajectory I

3.1.1 Coefficients

To transform the equation for the propagation of the coefficients it is far neater to use the notation of linear algebra as in equation (3.5) below:

$$\dot{\mathbf{C}}^{(I)} = \mathbb{X}_\nu^{(I)}\mathbf{C}^{(I)} = \left(\mathbb{X}_{eh,\nu}^{(I)} + \mathbb{X}_{qm,\nu}^{(I)}\right)\mathbf{C}^{(I)} \tag{3.5}$$

Where the $\mathbb{X}$ matrices are defined as in equations (3.6) and (3.7) below.

$$\mathbb{X}_{lk,\nu}^{eh(I)} = -\frac{i}{\hbar}E_l^{(I)} - \sum_\nu^{N_n} \frac{\mathbf{P}_\nu^{(I)}}{M_\nu} \cdot d_{lk,\nu}^{ad,(I)} \tag{3.6}$$

$$\mathbb{X}_{ll,\nu}^{qm(I)} = -\sum_{\nu=1}^{N_n} \sum_k \frac{\mathscr{Q}_{\nu,lk}^{(I)}}{\hbar M_{\nu'}} \cdot \left[\mathbf{f}_{k,\nu}^{(I)} - \mathbf{f}_{l,\nu}^{(I)}\right] |C_k^{(I)}|^2 \tag{3.7}$$

Using the identities:

$$\mathbb{U}^{-1} = \mathbb{U}^{\dagger} \tag{3.8}$$

$$\mathbf{C}^{(I)} = \mathbb{U}^{\dagger(I)}\mathbf{u}^{(I)} \tag{3.9}$$

$$\dot{\mathbf{C}}^{(I)} = \mathbb{U}^{\dot{\dagger}(I)}\mathbf{u}^{(I)} + \mathbb{U}^{\dagger(I)}\dot{\mathbf{u}}^{(I)} \tag{3.10}$$

Where $\mathbb{U}^{(I)} = \langle \phi_l^{(I)} | \psi_n^{(I)} \rangle$ is the unitary transformation matrix transforming from the diabatic to adiabatic basis. The $\mathbf{u}^{(I)}$ terms are the diabatic expansion coefficients on trajectory I.

After some algebra we arrive at:

$$\dot{\mathbf{u}}^{(I)} = \underbrace{\left(\mathbb{U}^{(I)}\mathbb{X}_{eh}\mathbb{U}^{\dagger(I)} + \mathbb{U}^{(I)}\mathbb{U}^{\dagger(I)}\right)\mathbf{u}^{(I)}}_{\text{Ehrenfest}} + \underbrace{\left(\mathbb{U}^{(I)}\mathbb{X}_{qm}\mathbb{U}^{\dagger(I)}\right)\mathbf{u}^{(I)}}_{\text{Quantum Momentum}} \tag{3.11}$$

In equation (3.11) I've separated the contribution from Ehrenfest and the contribution from the new quantum momentum terms. The Ehrenfest part can be shown to reduce to a simpler form (see Spencer, 2016[60] and Carof, 17[70] for more details). The quantum momentum term must be coded up as shown -with the transformation matrices. This gives the final equation for the propagation of the diabatic expansion coefficients, shown in equation (3.12).

$$\dot{\mathbf{u}}^{(I)} = \left(-\frac{i}{\hbar}\mathbb{H}^{(I)} - \mathbb{D}_{diab}^{(I)}\right)\mathbf{u}^{(I)} + \left(\mathbb{U}^{(I)}\mathbb{X}_{qm}\mathbb{U}^{(I)})^{-1}\right)\mathbf{u}^{(I)} \tag{3.12}$$

Where $\mathbb{H}^{(I)}$ is the diabatic Hamiltonian constructed via the AOM method, $\mathbb{D}_{diab}^{(I)}$ are the diabatic nonadiabatic coupling elements ($d_{diab,lk}^{(I)} = \langle \phi_l | \dot{\phi}_k \rangle$).

3.1.2 Forces

A full derivation of the transformation of basis for the equation propagating forces is given in appendix G. The result is given in equation (3.13) below:

$$\begin{aligned}\mathbf{F}^{(I)}_{eh,\nu} = &\sum_{i,j}\mathbf{u}^{*(I)}_{i}\mathbf{u}^{(I)}_{j}\left(\nabla_{\nu}H^{(I)}_{ij}+\sum_{l}\mathbf{d}^{(I)}_{lk,\nu}H^{(I)}_{lj}-\sum_{l}\mathbf{d}^{(I)}_{lj,\nu}H_{il}\right)\\ &-\sum_{l,k}|C^{(I)}_{l}|^{2}\left(\sum_{\nu'}^{N_n}\frac{2}{\hbar M_{\nu'}}\mathscr{Q}^{(I)}_{\nu',lk}\cdot\mathbf{f}^{(I)}_{l,\nu'}\right)\left[\mathbf{f}^{(I)}_{k,\nu}-\mathbf{f}^{(I)}_{l,\nu}\right]|C^{(I)}_{k}|^{2}\end{aligned} \tag{3.13}$$

There are a couple of things to note with this equation. Firstly, (as in the coefficients equation) the quantum momentum part has not been transformed. This is because the forces are basis independent and don't need to be transformed. Secondly, the quantities required for the calculation of this part of the equation are already calculated in order to propagate the coefficients so only a small amount of extra effort is required to calculate the quantum momentum force term. The Ehrenfest part of the equation has been transformed. This is because the nonadiabatic coupling vectors within the adiabatic basis are never required so are never calculated. The Ehrenfest force term requires these nonadiabatic coupling vectors so would add extra computational overheads. Further, the commutator term in the diabatic basis has been observed to provide a negligible contribution to the overall force in previous simulations (not shown in this work). This term requires significant computational effort and can be neglected. This makes the calculation of the Ehrenfest forces in the diabatic basis far cheaper than in the adiabatic basis.

3.2 Testing the diabatic propagator

The diabatic propagation can be tested against the already tested adiabatic propagator using the Tully model Hamiltonian. The code should give the same results, given the same inputs. To check this, in figure 3.1, the simulations carried out in figure 2.13 were repeated though this time the diabatic propagator was used. We can see in figure 3.1 that the results for the adiabatic and diabatic propagator are almost exactly the same for each model. In model 3, where the problem with the divergent $\mathscr{Q}^{(I)}_{lk,\nu}$ doesn't occur, the 2 results are exactly on top of each other. In the other models there is a slight discrepancy. This is due to the unpredictable $\mathscr{Q}^{(I)}_{lk,\nu}$ spikes not being perfectly corrected. However,

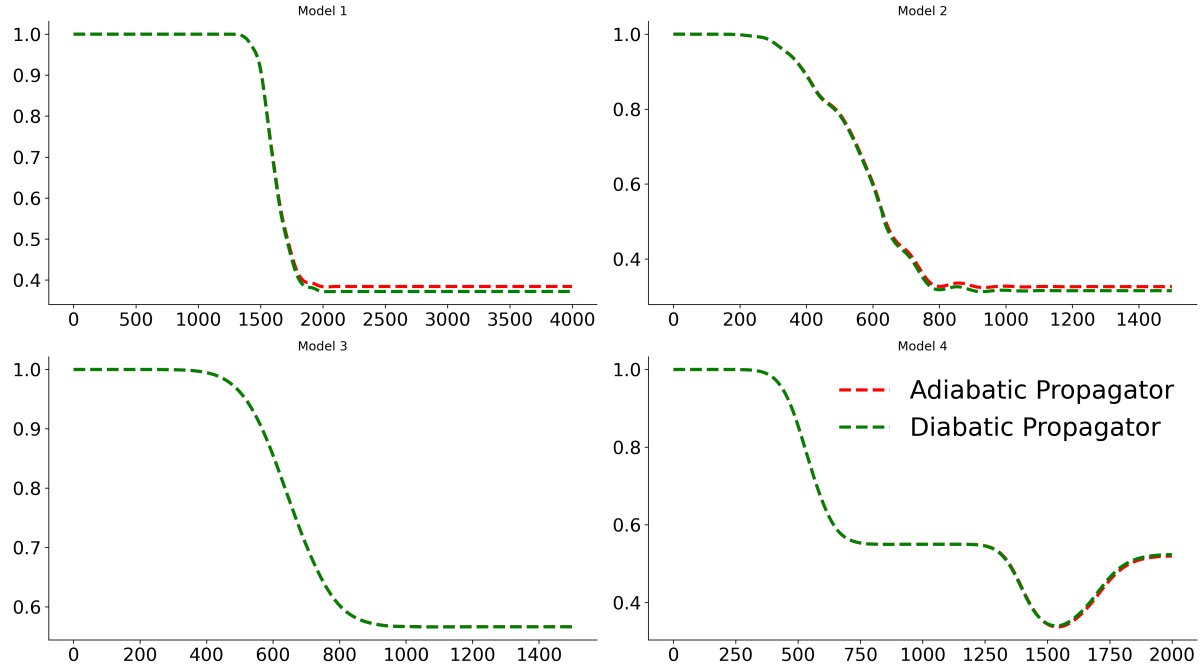

Figure 3.1: The 4 Tully models simulated using propagating the equations within a diabatic and adiabatic basis. The green line shows results from the diabatic propagator and the red line shows results from the adiabatic propagator. Model 3 shows an exact agreement between the adiabatic and diabatic propagators hence only 1 line is seen.

figure 3.1 still serves as confirmation of the propagation within the diabatic basis.

3.3 Simulating Molecular Systems

To go beyond the 1D Tully model systems the AOM method is combined with CTMQC and applied to an Ethylene dimer. Fortunately, the majority of the code from the Tully model systems can be re-used. In fact, the only difference is the way the Hamiltonian (and diabatic NACE) is constructed. The code for carrying out these tasks (the AOM part) has been implemented by previous members of the group and has been well tested and verified against the literature and experimental studies. Therefore, I will not include any tests of this part of the code in this document but instead refer the reader to the numerous papers discussing AOM and its use in within the fewest switches surface hopping framework[14,69,71–79]. An ethylene dimer was chosen as a reasonable first system due to its relative simplicity (shown in figure 3.2) the total number of atoms is 12 and only 2 electronic states will be considered. The system shown in figure 3.2 was initialised in the adiabatic ground state. Positions and velocities were sampled from a short NVT

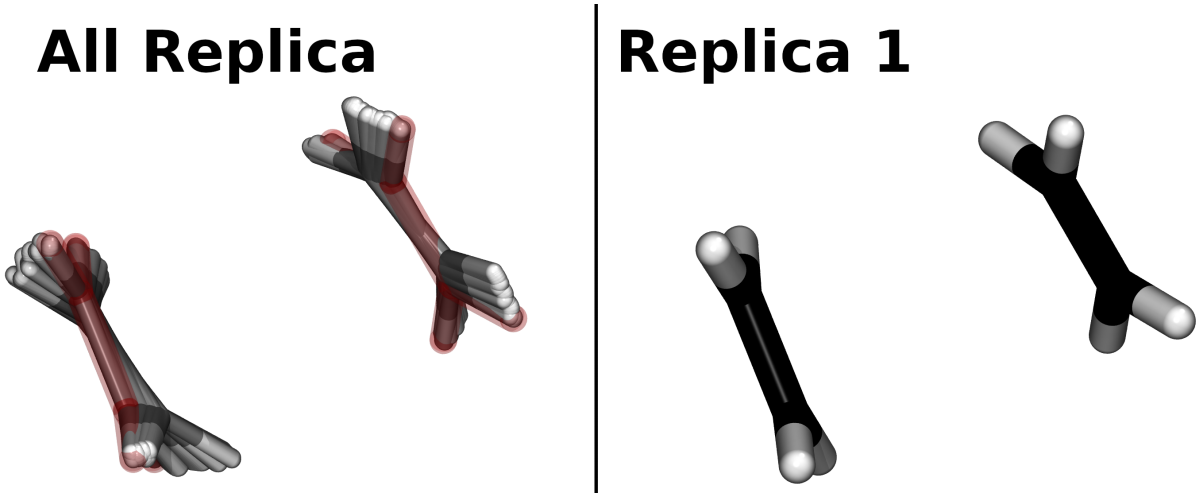

Figure 3.2: An example Ethylene dimer used to test the CTMQC implementation. The right panel shows the positions of just 1 replica. The left panel shows the positions of all replica with the replica shown on the right highlighted in red.

molecular dynamics equilibration. The scaling factor (C in equation (3.1)) was chosen to give a coupling of approximately 27 meV. This is approximately $\frac{1}{4}\times$ the reorganisation energy -parameterised to be 100 meV. The amount of charge transfer is dependent on the ratio between reorganisation energy and the electronic couplings ($\frac{H_{ab}}{\lambda}$). The factor of $\frac{1}{4}$ was chosen to be a reasonable factor -seen in other organic semiconducting systems. The nuclear timestep was chosen to be 0.05fs and the electronic one was 0.005 fs. The switch to $\mathbf{R}^{(I)}_{0,\nu}$ was chosen as the correction method of the quantum momentum and 100 trajectories were used. A constant σ of 0.7 was used as the dynamic σ tended to either vanish to 0 or blow up to a very large number.

In figure 3.3 the norm of the diabatic expansion coefficients are plotted, from the system described above. In this figure we see large jumps in the norm, these are caused by the divergences in the quantum momentum term. These occur more in this system than in the Tully models as it is more complex (more atoms, higher dimensional) and runs for a longer time with more avoided crossings. The fact that there are 12 atoms and 3 Cartesian dimensions instead of 1 means that the $\mathbf{R}_{lk,\nu}$ term must be calculated many more times increasing the probability of happening upon a divergence. For example, the Tully models tended to run for 10s of fs and had 1 value of $\mathbf{R}_{lk,\nu}$. The Ethylene dimer typically runs for 100s of fs encountering 10s of avoided crossings with 36 unique values

of $\mathbf{R}_{lk,\nu}$. The errors can also accumulate meaning that after a few trivial crossings the populations become extremely noisy. This eventually causes the code to crash and results from it cannot be trusted. Most commonly the reason for the code crashing is a large spike in the computed forces caused by a spike in the quantum momentum. This large force then causes the atoms to collide and the code to crash. The code is very stable when just using Ehrenfest dynamics. Many more simulations have been carried out to

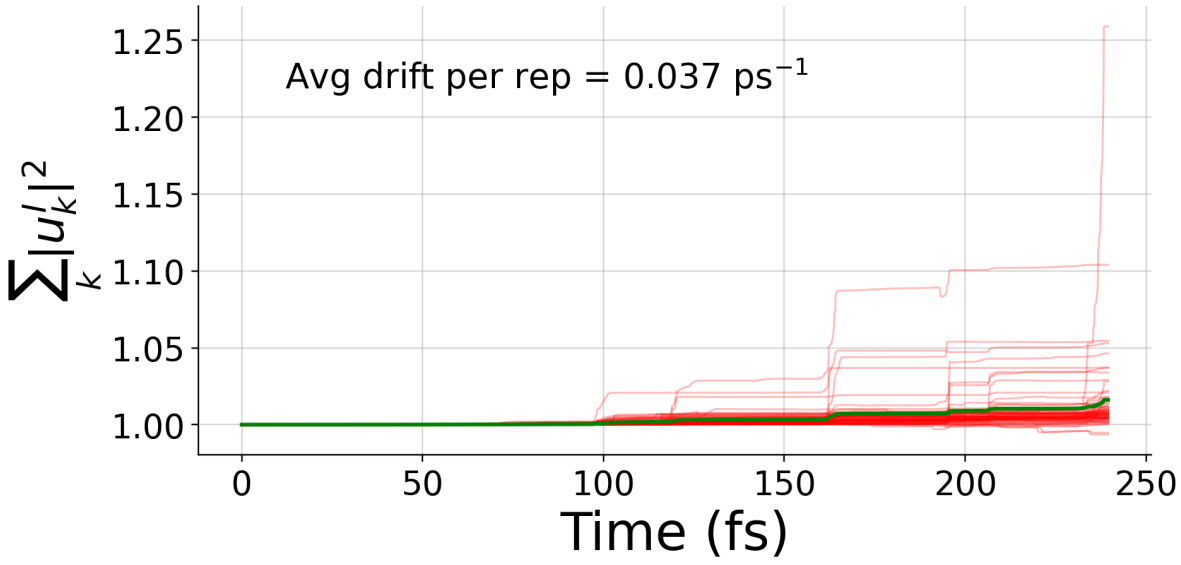

Figure 3.3: The norm of the adiabatic expansion coefficients. Thin red lines show the norm for each trajectory and the thick green line shows the average over all trajectories.

diagnose and fix this issue. Results from all of these cannot be included in this document though I will provide a brief summary of results below.

- Varying the number of replicas: Increasing the number of replicas in the system, somewhat counterintuitively, decreases stability. This is because with more replicas there is more of a chance the code will stumble upon a calculation giving a divergence in the quantum momentum term.

- Varying the timestep: Decreasing the timestep does help to improve norm conservation (before the code crashes). However, it does not lead to a more stable simulation that allows for longer timescales to be simulated. This is because decreasing the

timestep provides more opportunity for a small numerical error to cause a divergence in the quantum momentum term.

- Removing Center of Mass Motion: In some simulations the replicas positions spread out so much that the quantum momentum term became negligible. This was to prevent that from happening.

- Varying the gaussian width (σ) parameter: If the σ parameter is set to be large ($>$ 2) then the simulation is more stable as the quantum momentum term is smaller and errors don't accumulate as quickly. However, this the limit of a very large σ is Ehrenfest dynamics. If the σ is set to be small (< 0.2) the simulation becomes extremely unstable as the quantum momentum forces populations to decohere too quickly. This is discussed in more detail in section 2.3.

- Turning off the quantum momentum addition to the force term: The code runs more stably if the quantum momentum term is not included in the forces. This has also been shown to be much less important for the accuracy of the results than the quantum momentum addition to the coefficients. However, even in this case the code eventually crashes after an accumulation of errors in the coefficients results in erroneous forces resulting in geometries that fail CP2K internal checks.

- Renormalisation: This does not seem to help with stability. Furthermore, it merely helps hide the large norm drift and doesn't fix the problems it causes.

3.4 Conclusions

The CTMQC method shows great promise as a new nonadiabatic molecular dynamics (NAMD) technique. It was derived as the semi-classical limit of the exact factorisation of the time-dependent electron-nuclear wave function[47,48]. It purports to handle decoherence corrections in a more rigorous, first principles way without the need of empirical parameters. Although this method was first reported in 2015[48], there are still very few papers reporting results using this method[3,48,56]. With the most complex system being restricted to a 7 atom molecule simulated for just 10s of fs[56]. In this work, I have transformed the basis of the CTMQC equations, to an orthogonal diabatic basis, and

implemented it within the FOB framework. This has allowed me to study to a molecular system (dimer of Ethylene) totalling 12 atoms, simulated for hundreds of fs. However, instabilities in the algorithm have prevented any physical conclusions being drawn from this. Before, the widespread acceptance of CTMQC as a standard nonadiabatic molecular dynamics method 2 critical flaws must be addressed. First is the calculation of the gaussian width parameter, σ and the second is the divergence of the quantum momentum term. It would be possible to further investigate the width parameter, perhaps through benchmarks against higher level calculations to establish a relationship between it and other characteristics of the system. From a short investigation using the Tully models it seems a constant width parameter gives reasonable results and it should be set to be between 0.2 and 0.5. The on-the-fly algorithm provided even better results and would probably be a good choice in most simulations. The setting of this parameter does not seem like an intractable problem. However, it may be harder to correct for the large divergences in the quantum momentum caused by the denominator of the quantum momentum intercept term, $\mathbf{R}_{lk,\nu}$, approaching zero. This causes the code to become unstable for even simple molecular systems. In the 1D Tully models this could be corrected by switching to an alternative intercept, $\mathbf{R}^{(I)}_{0,\nu}$. However, this alternative intercept results in unphysical population transfer in regions of zero nonadiabatic coupling, so cannot be used throughout the simulation. The Tully models also gave fewer divergences due to smaller run-times and the fact it is a simpler system. For any larger, more complex, systems the correction soon starts to fail preventing any reasonable physical conclusions being drawn.

Both these problems can both be traced back to the construction of the nuclear density from the nuclear positions. The method explored in this thesis is the method reported in the literature. That involves placing a gaussian function centered on each atomic position with a certain width, σ to smear out the (point) position and give a smooth nuclear distribution. I believe that exploring alternative techniques to construct the nuclear density from atomic positions may lead to the largest improvements in the CTMQC technique. Perhaps even allowing one to study complex molecular systems with many nonadiabatic coupling regions such as those typically found in charge transfer studies.

To address the 2 aforementioned problems I have given solutions that work well for the simple Tully systems. To address the sudden divergence of the quantum momentum term, I have presented an algorithm for smoothing out large divergences (based on a gradient threshold) which improves norm conservation substantially. However, for more complex systems the smoothing correction does not seem to be enough and errors soon accumulate. To address the uncertainty in the width parameter for constructing the nuclear density, I have investigated various constant values of the width parameter and a method to dynamically update it on-the-fly (taken from Gossel[3]). The dynamic update worked well for the Tully models bringing CTMQC results very close to the exact results. However, due to instabilities in the algorithm, it wasn't possible to investigate reasonable values of $\boldsymbol{\sigma}$ for molecular systems. Finally, the current formulation of the algorithm does not seem to conserve total energy. Using the equation for potential energy given in[48] we see that even very small nuclear timesteps do not conserve total energy to less than 10^{-2} Ha ps^{-1} atom^{-1} in the best case. For reference, a good energy conservation within classical molecular dynamics is considered to be $\sim 10^{-10}$ or less. Further, and perhaps more concerning, reducing the timestep does not seem to improve the issue. This would be a major obstacle to CTMQC's widespread adoption as a nonadiabatic molecular dynamics algorithm. In the rest of this work I will discuss an alternative NAMD technique, namely fewest switches surface hopping (FSSH), and apply it to large molecular systems to get experimentally verifiable results.

I have implemented and tested a working version of CTMQC both in CP2K and as a standalone python script. These are both available for downloading from the author's github page at: https://github.com/95ellismle. I

Appendix A

Tully Model Paramters

A.1 Model 1 -Single Avoided Crossing

Hamiltonian Paramters:

$$H_{11}(\mathbf{R}) = A \tanh(B\mathbf{R})$$
$$H_{12}(\mathbf{R}) = Ce^{-D\mathbf{R}^2}$$
$$H_{21}(\mathbf{R}) = H_{12}(\mathbf{R})$$
$$H_{22}(\mathbf{R}) = -H_{11}(\mathbf{R})$$

Where A = 0.03, B = 0.4, C = 0.005 and D = 0.3

Quantity	Value	Unit
Initial Position	-20	a.u.
Initial Velocities	15.0, 25.0	a.u.
Initial Adiab Pop	ground state	-
Simulation Time	6000, 4000	a.u.
$\sigma_v^{(I)}$	0.5	a.u.
M (σ constant)	40	-
$\Delta t_{\text{nuclear}}$	0.1	fs
$\Delta t_{\text{electonic}}$	0.01	fs
$\frac{\delta \mathbf{R}_{lk,v}^{(I)}}{\delta t}$ threshold	0.15	a.u.
N_{rep}	200	-

A.2 Model 2 -Dual Avoided Crossing

Hamiltonian Paramters:

$$H_{11}(\mathbf{R}) = 0$$
$$H_{12}(\mathbf{R}) = Ce^{-D\mathbf{R}^2}$$
$$H_{21}(\mathbf{R}) = H_{12}(\mathbf{R})$$
$$H_{22}(\mathbf{R}) = -Ae^{-B\mathbf{R}^2} + E$$

Where A = 0.1, B = 0.28, C = 0.015, D = 0.06 and E = 0.05

Quantity	Value	Unit
Initial Position	-8	a.u.
Initial Velocities	16.0, 30.0	a.u.
Initial Adiab Pop	ground state	-
Simulation Time	2500, 1500	a.u.
$\sigma_\nu^{(I)}$	0.5	a.u.
M (σ constant)	40	-
$\Delta t_{\text{nuclear}}$	0.1	fs
$\Delta t_{\text{electonic}}$	0.01	fs
$\frac{\delta \mathbf{R}_{lk,\nu}^{(I)}}{\delta t}$ threshold	0.15	a.u.
N_{rep}	200	-

A.3 Model 3 -Extended Coupling

Hamiltonian Paramters:

$$H_{11}(\mathbf{R}) = A$$
$$H_{12}(\mathbf{R}) = \begin{cases} Be^{C\mathbf{R}}, & R \leq 0 \\ B(2 - e^{-C\mathbf{R}}), & R > 0 \end{cases}$$
$$H_{21}(\mathbf{R}) = H_{12}(\mathbf{R})$$
$$H_{22}(\mathbf{R}) = -H_{11}(\mathbf{R})$$

Where A = 6×10^{-4}, B = 0.1 and C = 0.9

Quantity	Value	Unit
Initial Position	-15	a.u.
Initial Velocities	10, 30	a.u.
Initial Adiab Pop	ground state	-
Simulation Time	5000, 1500	a.u.
$\sigma_\nu^{(I)}$	0.5	a.u.
M (σ constant)	40	-
$\Delta t_{\text{nuclear}}$	0.1	fs
$\Delta t_{\text{electonic}}$	0.01	fs
$\frac{\delta \mathbf{R}_{lk,\nu}^{(I)}}{\delta t}$ threshold	0.15	a.u.
N_{rep}	200	-

A.4 Model 4 -Dual Arch

Hamiltonian Paramters:

$$H_{11}(\mathbf{R}) = A$$

$$H_{12}(\mathbf{R}) = \begin{cases} B\left[-e^{C(\mathbf{R}-D)} + e^{C(\mathbf{R}+D)}\right] & R \leq -D \\ B\left[e^{-C(\mathbf{R}-D)} - e^{-C(\mathbf{R}+D)}\right] & R \geq D \\ B\left[2 - e^{C(\mathbf{R}-D)} - e^{-C(\mathbf{R}+D)}\right] & -D < R < D \end{cases}$$

$$H_{21}(\mathbf{R}) = H_{12}(\mathbf{R})$$

$$H_{22}(\mathbf{R}) = -H_{11}(\mathbf{R})$$

Where A = $6\times\ 10^{-4}$, B = 0.1, C = 0.9 and D = 4

Quantity	Value	Unit
Initial Position	-20	a.u.
Initial Velocities	10, 40	a.u.
Initial Adiab Pop	ground state	-
Simulation Time	6000, 2000	a.u.
$\sigma_{\nu}^{(I)}$	0.5	a.u.
M (σ constant)	40	-
$\Delta t_{\text{nuclear}}$	0.1	fs
$\Delta t_{\text{electonic}}$	0.01	fs
$\frac{\delta \mathbf{R}_{Ik,\nu}^{(I)}}{\delta t}$ threshold	0.15	a.u.
N_{rep}	200	-

Appendix B

Wigner Distribution Derivation

The nuclear wavepacket (at time 0) is given by:

$$\chi(R) = \frac{1}{(\pi\mu^2)^{\frac{1}{4}}} e^{-\frac{(R-R_0)^2}{2\mu^2} + ik_0(R-R_0)} \tag{B.1}$$

The Wigner quassiprobability function for momentum and position (p, R) is given by:

$$W(p,R) = \frac{1}{\pi\hbar} \int_{-\infty}^{\infty} \chi^*(R+y)\chi(R-y)e^{\frac{2ipy}{\hbar}} dy \tag{B.2}$$

However, both Ehrenfest and CTMQC require atomic positions as input so we must extract the position and velocity probability densities from this. We get these from the marginal integrals of the Wigner distribution i.e.

$$|f(R)|^2 = \int_{-\infty}^{\infty} W(R,p)dp \tag{B.3}$$

$$|f(p)|^2 = \int_{-\infty}^{\infty} W(R,p)dR \tag{B.4}$$

In order to calculate these marignal integrals we must first crunch through the maths of equation (B.2). Substituting eq (B.1) into (B.2):

$$W(p,R) = \frac{1}{\pi\hbar} \int_{-\infty}^{\infty} \frac{1}{\mu\sqrt{\pi}} e^{-\frac{(R+y-R_0)^2}{2\mu^2} - 2ik_0y - \frac{(R-y-R_0)^2}{2\mu^2}} e^{\frac{2ipy}{\hbar}} dy \tag{B.5}$$

Simplifying the 2 quadratic equations (equation (B.5)) we get:

$$W(p,R) = \frac{1}{\pi\hbar}\int_{-\infty}^{\infty} \frac{1}{\mu\sqrt{\pi}} e^{-\mu^{-2}\left(y^2 - 2ik_0 y\mu^2 + (R-R_0)^2\right)} e^{\frac{2ipy}{\hbar}} dy \tag{B.6}$$

We can now take the expressions not dependant on y outside of the integral and combine the exponents.

$$W(p,R) = \frac{1}{\pi\sqrt{\pi}\mu\hbar} e^{-\frac{(R-R_0)^2}{\mu^2}} \int_{-\infty}^{\infty} e^{-\frac{y^2 + 2iy\mu^2\left(\frac{p}{\hbar} - k_0\right)}{\mu^2}} dy \tag{B.7}$$

Integrating we get:

$$\int e^{-\frac{y^2 + 2iy\mu^2\left(\frac{p}{\hbar} - k_0\right)}{\mu^2}} dy = \frac{\sqrt{\pi}\mu}{2} e^{-\frac{\mu^2}{\hbar^2}(p - \hbar k_0)^2} erf\left[\frac{y}{\mu} + i\left(\frac{p\mu}{\hbar} - \mu k_0\right)\right] \tag{B.8}$$

Applying limits we get:

$$\int_{-\infty}^{\infty} e^{-\frac{y^2 + 2iy\mu^2\left(\frac{p}{\hbar} - k_0\right)}{\mu^2}} dy = \sqrt{\pi}\mu e^{-\frac{\mu^2}{\hbar^2}(p - \hbar k_0)^2} \tag{B.9}$$

Substituting this back into the Wigner distribution (equation (B.2)) we finally get:

$$W(p,R) = \frac{1}{\pi\hbar} e^{-\frac{(R-R_0)^2}{\mu^2}} e^{-\frac{(p - \hbar k_0)^2}{\hbar^2/\mu^2}} \tag{B.10}$$

Taking the maringal integrals we get the position and velocity probability distributions:

$$|f(R)|^2 = \frac{2}{\mu\sqrt{\pi}} e^{-\frac{(R-R_0)^2}{\mu^2}} \tag{B.11}$$

$$|f(p)|^2 = \frac{2}{\frac{\hbar}{\mu}\sqrt{\pi}} e^{-\frac{\mu^2}{\hbar^2}(p - \hbar k_0)^2} \tag{B.12}$$

The above distributions are randomly sampled to get initial atomic velocities and positions for each simulation.

Appendix C

$\mathbf{R}_{lk,\nu}$ Alternatives

C.1 $\mathbf{R}_{lk,\nu}$ Extrapolation

C.2 Alternative Quantum Momentum Intercept

In Agostini, 16[2] another quantum momentum intercept term is discussed. This term is not used because, as previously discussed in section 1.4, it leads to unphysical transfer of population between adiabatic states when the nonadiabatic coupling elements are 0. However, it can be used in these Tully Models as an effective fix to the discontinuities caused by the $\mathbf{R}_{lk,\nu}$ term.

The other quantum momentum intercept, $\mathbf{R}^{(I)}_{0,\nu}$, comes directly from the construction of the nuclear density using a linear combination of a product of gaussians (see equation (1.12) in the introduction). It is defined as in equation (C.1) below:

$$\mathbf{R}^{(I)}_{0,\nu} = \sum_{J}^{N_{tr}} \left[\frac{\hbar \prod_{\nu'} g_{\sigma^{(J)}_{\nu'}(t)} \left(\mathbf{R}^{(I)}_{\nu'}(t) - \mathbf{R}^{(J)}_{\nu'}(t) \right)}{2\sigma^{(J)}_{\nu}(t)^2 \sum_{K}^{N_{tr}} \prod_{\nu'} g_{\sigma^{(K)}_{\nu'}(t)} \left(\mathbf{R}^{(I)}_{\nu'}(t) - \mathbf{R}^{K)}_{\nu'}(t) \right)} \mathbf{R}^{(I)}_{\nu} \right] \tag{C.1}$$

However, as switching to this intercept directly may cause discontinuities in itself a smoothing parameter is applied to ease the switch. This is given in equation (C.2) below:

$$[1 - A(t)] R_{good}(t) + A(t) R_{bad}(t) = R_{effective}(t) \tag{C.2}$$

R_{good} refers to the intercept that should be switched to (e.g. for the detection of a spike in the $R^{(I)}_{lk,\nu}$ we switch to the intercept in in equation (C.1)). $R^{(I)}_{lk,\nu}$ refers to the intercept that is being switched from (e.g. when it is detected that the divergence of $R^{(I)}_{lk,\nu}$ has finished then we switch from the alternative intercept back to $R^{(I)}_{lk,\nu}$). $A(t)$ is a smoothing parameter and is given in equation (C.3) below:

$$A(t) = \frac{D^{(I)}_{\nu}}{2}\left[tanh\left(t - \frac{t_{final}+t_{init}}{0.6Ndt}\right)+1\right] \tag{C.3}$$

Where $D^{(I)}_{\nu}$ is the distance between the 2 intercepts (e.g. $D^{(I)}_{\nu} = R^{(I)}_{lk,\nu} - R^{(I)}_{0,\nu}$), N is the number of steps to take before settling solely on one intercept, t_{init} is the time of detection of the divergence, t_{final} is the time at which the code settles on 1 intercept and dt is the timestep taken.

A cartoon of this process is given in figure C.1

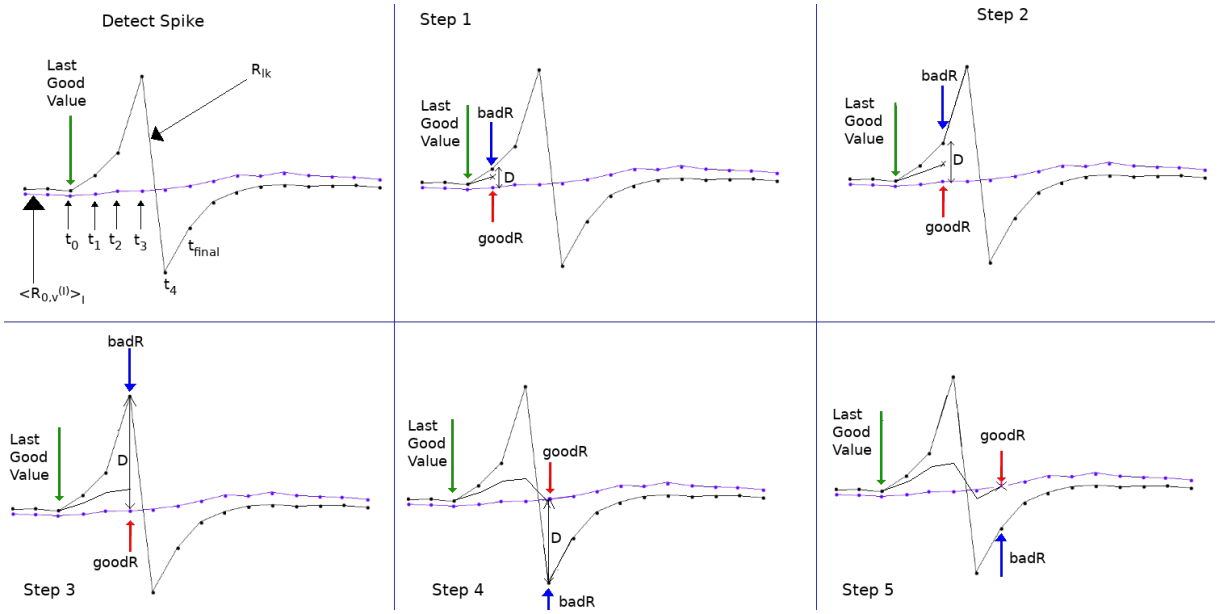

Figure C.1: A crude demonstration of the principle behind the smoothing procedure in switching between intercepts. The black line shows an intercept begin to diverge and the alternative intercept is shown in purple. As the step is incremented the amount of the alternative intercept that makes up the effective intercept is increased until only 1 intercept is used.

Appendix D

Rabi Oscillation

The time dependant Schrödinger equation is given below:

$$i\hbar\frac{\delta}{\delta t}\Phi(\mathbf{R}(t),t) = \hat{H}(\mathbf{R}(t),t)\Phi(\mathbf{R}(t),t) \tag{D.1}$$

If we hold the nuclear coordinates in place (e.g. remove time-dependence from nuclear coordinates) we get an ordinary differential equation as shown below:

$$i\hbar\frac{d}{dt}\Phi(\mathbf{R},t) = \hat{H}(\mathbf{R},t)\Phi(\mathbf{R},t) \tag{D.2}$$

This has the following general solution. This can be solved with a Taylor series expansion.

$$\Phi(\mathbf{R},t) = e^{i\hbar\hat{H}t}\Phi(\mathbf{R},0)$$

Figure

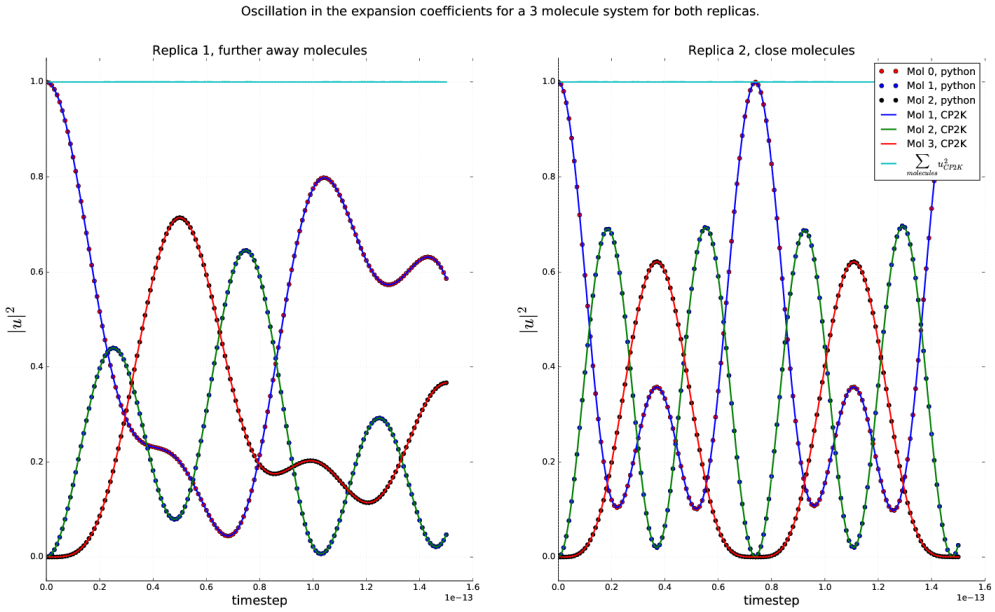

Figure D.1: Rabi oscillation occurring within a Ethylene trimer system. Dotted lines were calculated using equation (D.2), solid lines were calculated using the RK4 propagator within the CTMQC section of the CP2K code. The norm is shown on the top as a cyan line and the x axis shows the timestep in seconds.

Appendix E

Norm Conservation in CTMQC and Ehrenfest

A statement of the conservation of the norm, for a single trajectory, is given below in equation (E.1)

$$\frac{d}{dt}\sum_l |C_l(t)|^2 = \sum_l C_l^*(t)\frac{dC_l(t)}{dt} + \frac{dC_l^*(t)}{dt}C_l(t) = 2\mathbb{R}\left[\sum_l C_l(t)^*\frac{dC_l(t)}{dt}\right] \tag{E.1}$$

Substituting the equation for the evolution of the adiabatic coefficients (and removing the purely imaginary term) into (??) we get equation (E.3)

$$\frac{d}{dt}\sum_l |C_l(t)|^2 = 2\sum_l \mathbb{R}\left[\cancel{\frac{-i}{\hbar}\varepsilon^l_{BO}C_l(t)^*C_l(t)} - \sum_k \left[C_l(t)^*C_k(t)d^{ad}_{lk} - (A_l - B_l)C_l(t)^*C_l(t)\right]\right] \tag{E.2}$$

$$= -2\sum_l \mathbb{R}\left[\sum_k \left[C_l(t)^*C_k(t)d^{ad}_{lk} - (A_l - B_l)C_l(t)^*C_l(t)\right]\right] \tag{E.3}$$

Where:

$$A_l = \sum_{\nu=1}^{N_n}\sum_k \frac{\mathscr{Q}_{lk,\nu}(t)}{\hbar M_\nu}\cdot \mathbf{f}_{k,\nu}(t)|C_k(t)|^2 \tag{E.4}$$

$$B_l = \sum_{\nu=1}^{N_n}\sum_k \frac{\mathscr{Q}_{lk,\nu}(t)}{\hbar M_\nu}\cdot \mathbf{f}_{l,\nu}(t)|C_k(t)|^2 \tag{E.5}$$

The NACE term evaluates to 0 due to the anti-symmetry of the NACE giving us equation (E.7).

So far, we have proved that the norm should be conserved here for all terms apart from the quantum momentum terms i.e. Ehrenfest.

$$\frac{d}{dt}\sum_l \left|C_l^{QM}(t)\right|^2 = 2\sum_l \mathbb{R}\left[(A_l - B_l)C_l(t)^* C_l(t)\right] \tag{E.6}$$

$$= 2\left[\sum_l A_l |C_l(t)|^2 - \sum_l B_l |C_l(t)|^2\right] \tag{E.7}$$

However, $\sum_l A_l|C_l|^2 \equiv \sum_l B_l|C_l|^2$, therefore there is no change in the population and the norm should be conserved.

Appendix F

Dynamic $\boldsymbol{\sigma}$ Calculation

The algorithm for dynamically updating the σ parameter outlined in Gossel, 18[3] is provided below.

1. Set an initial width parameter $(\sigma_\nu^{(I)}(t-dt))$ and a constant we will name D.
2. Calculate a cutoff distance via: $r_{cut}(t) = D\sigma_\nu^{(I)}(t-dt)$.
3. For each atom index, ν, and replica, I, gather replicas within a cutoff distance of the current replica. Set the number of replicas within the cutoff distance to N.
4. Calculate the distance between atoms on different replicas.
5. Find the standard deviation of these distances and set the width of the gaussian, centered on atom ν and replica I, to this standard deviation.
6. If the standard deviation is smaller than $\frac{D}{N} min_I \left[\sigma_\nu^{(I)}(t-dt)\right]$ then set $\sigma_\nu^{(I)}(t) = \frac{D}{N} min_I \left[\sigma_\nu^{(I)}(t-dt)\right]$.

Appendix G

Basis Transformation

We can expand the Schrödinger equation in terms of a diabatic basis, ϕ rather than an adiabatic one, ψ. These 2 expansions are given in equations (G.1) and (G.2).

$$|\Psi\rangle = \sum_n C_n |\psi_n\rangle \tag{G.1}$$

$$|\Psi\rangle = \sum_l u_l |\phi_l\rangle \tag{G.2}$$

It follows from this we can define a transformation matrix, U_{ln} to transform between the adiabatic and diabatic bases. This is shown in equation (G.3) where the $\overleftrightarrow{I}$ symbol represents the identity matrix. This identity only holds in the orthogonal diabatic basis ϕ and wouldn't hold for non-orthogonal bases.

$$|\psi_n\rangle = \overleftrightarrow{I}\,|\psi_n\rangle = \sum_l |\phi_l\rangle\langle\phi_l|\,\psi_n\rangle = \sum_l |\phi_l\rangle U_{ln} \tag{G.3}$$

A similar relation between expansion coefficients exists

$$\sum_n C_n |\psi_n\rangle = \sum_l u_l |\phi_l\rangle \tag{G.4}$$

$$\sum_n C_n \langle\psi_m|\psi_n\rangle = \sum_l u_l \langle\psi_m|\phi_l\rangle \tag{G.5}$$

$$C_m = \sum_l u_l U^*_{lm} \tag{G.6}$$

Finally an important property of the transformation matrix is given in equation (G.7).

$$\sum_m U_{im} U_{lm}^* = \sum_m \langle \phi_i | \psi_m \rangle \langle \psi_m | \phi_l \rangle = \langle \phi_i | \phi_l \rangle = \delta_{il} \tag{G.7}$$

Equations (G.3), (G.6) and (G.7) will be used below to transform the propagation equations from the adiabatic basis to the diabatic one.

G.1 Forces

The equation for the propagation of the forces in the adiabatic basis is:

$$\begin{aligned} \mathbf{F}_\nu^{(I)} = &- \sum_n |C_n^{(I)}|^2 \nabla_\nu E_n^{(I)} - \sum_{n,m} C_m^{*(I)} C_n^{(I)} \left(E_n^{(I)} - E_m^{(I)} \right) \mathbf{d}_{\nu,mn}^{ad,(I)} \\ &- \sum_{m,n} |C_m^{(I)}|^2 \left(\sum_{\nu'}^{N_n} \frac{2}{\hbar M_{\nu'}} \mathscr{Q}_{\nu',mn}^{(I)} \cdot \mathbf{f}_{m,\nu'}^{(I)} \right) \left[\mathbf{f}_{n,\nu}^{(I)} - \mathbf{f}_{m,\nu}^{(I)} \right] |C_n^{(I)}|^2 \end{aligned} \tag{G.8}$$

The quantum momentum part of the equation cannot be easily transformed so this will focus on the Ehrenfest part:

$$\mathbf{F}_{eh,\nu}^{(I)} = - \sum_n |C_n^{(I)}|^2 \nabla_\nu E_n^{(I)} - \sum_{n,m} C_m^{*(I)} C_n^{(I)} \left(E_n^{(I)} - E_m^{(I)} \right) \mathbf{d}_{\nu,mn}^{ad,(I)} \tag{G.9}$$

Using equation (10) in Carof, 17[70] and the Hellman-Feynman theorem we can rewrite equation (G.9) as equation (G.10):

$$\mathbf{F}_{eh,\nu}^{(I)} = \sum_{m,n} C_m^{*(I)} C_n^{(I)} \langle \psi_m | \nabla_\nu H | \psi_n \rangle \tag{G.10}$$

We can substitute the coefficients and basis functions for those in equations (G.3) and (G.6). This carried out in equation (G.15). However, I have removed the trajectory and

atom index from the terms to make the notation clearer.

$$F_{eh,\nu} = \sum_{m,n} C_m^* C_n \langle \psi_m | \nabla_H | \psi_n \rangle \tag{G.11}$$

$$= \sum_{m,n} \sum_i u_i^* U_{im} \sum_j u_j U_{jn}^* \sum_l U_{lm}^* \sum_k U_{kn} \langle \phi_l | \nabla H | \phi_k \rangle \tag{G.12}$$

$$= \sum_{m,n} \sum_{i,j,k,l} u_i^* u_j U_{im} U_{lm}^* U_{jn}^* U_{kn} \langle \phi_l | \nabla H | \phi_k \rangle \tag{G.13}$$

$$= \sum_{i,j,k,l} u_i^* u_j \delta_{il} \delta_{jk} \langle \phi_l | \nabla H | \phi_k \rangle \tag{G.14}$$

$$= \sum_{i,j} u_i^* u_j \langle \phi_i | \nabla H | \phi_j \rangle \tag{G.15}$$

However, in the code the expectation value of the gradient of the Hamiltonian ($\langle \phi_i | \nabla H | \phi_j \rangle$) isn't very easily calculable. However, the gradient of the Hamiltonian matrix elements ($\nabla \langle \phi_i | H | \phi_j \rangle$) is easily calculable via the overlap term, $\nabla H = C \nabla S_{ij}$. Therefore, using chain rule we can re-write equation (G.15) as:

$$F_{eh,\nu} = \sum_{i,j} u_i^* u_j \langle \phi_i | \nabla H | \phi_j \rangle \tag{G.16}$$

$$= \sum_{i,j} u_i^* u_j \left(\nabla \langle \phi_i | H | \phi_j \rangle - \langle \nabla \phi_i | H | \phi_j \rangle - \langle \phi_i | H | \nabla \phi_j \rangle \right) \tag{G.17}$$

$$= \sum_{i,j} u_i^* u_j \left(\nabla \langle \phi_i | H | \phi_j \rangle - \sum_l \langle \nabla \phi_i | \phi_l \rangle \langle \phi_l | H | \phi_j \rangle - \sum_l \langle \phi_i | H | \phi_l \rangle \langle \phi_l | \nabla \phi_j \rangle \right) \tag{G.18}$$

$$= \sum_{i,j} u_i^* u_j \left(\nabla \langle \phi_i | H | \phi_j \rangle + \sum_l \mathbf{d}_{il} \langle \phi_l | H | \phi_j \rangle - \sum_l \mathbf{d}_{lj} \langle \phi_i | H | \phi_l \rangle \right) \tag{G.19}$$

Giving the final equation for the transformed forces as:

$$\mathbf{F}_{eh,\nu}^{(I)} = \sum_{i,j} \mathbf{u}_i^{*(I)} \mathbf{u}_j^{(I)} \left(\nabla_\nu H_{ij}^{(I)} + \sum_l \mathbf{d}_{lk,\nu}^{(I)} H_{lj}^{(I)} - \sum_l \mathbf{d}_{lj,\nu}^{(I)} H_{il} \right) \tag{G.20}$$

Appendix H

Adiabatic State Initialisation

By diagonalising the Hamiltonian we get the adiabatic energies (eigenvalues) for each state and transformation matrix (eigenvectors) to calculate diabatic states $\mathbb{U}$. We can calculate diabatic coefficients corresponding to each adiabatic state via equation (H.1) below.

$$\mathbb{U}\mathbf{C}_n = \mathbf{u}_n \tag{H.1}$$

Where $\mathbb{U}$ is the transformation matrix of size (N_{mol}, N_{mol}), $\mathbf{C}$ is a complex vector of size N_{mol} containing coefficients for adiabatic state n and $\mathbf{u}$ is a complex vector of size N_{mol} containing coefficients for diabatic state n.

Seeing as we would like to find the diabatic population corresponding to each adiabatic state we localise coefficients on each pure adiabatic state and carry out the transformation e.g: $C_i = (1+0i, 0+0i, 0+0i, ...)$ when we want to find the diabatic coefficient corresponding to state 1 and $C_i = (0+0i, 1+0i, 0+0i, ...)$ when we want to find the diabatic coefficient corresponding to state 2 etc.. Therefore, the column, n, of the transformation matrix, $\mathbb{U}$, gives the diabatic coefficients corresponding to adiabatic state, n, as shown below in equation (H.2)

$$U_{in} = u_i \tag{H.2}$$

Where n is the adiabatic state index and i is the diabatic (molecular) state index.

Once we have the diabatic state corresponding to each adiabatic state, and the en-

ergy of that adiabatic state, we can find which state best fulfills the requirements of being close to the center of the system and being within 3KT of the ground state. In order to do this, we can loop over each adiabatic state in increasing order of energy. The center of the system is calculated and the population weighted average center of mass, $\mathbf{R}_n$ of the diabatic coefficients corresponding to adiabatic state n is calculated as in equation (H.3).

$$\mathbf{R}_n = \sum_i |u_i|^2 \mathbf{R}_{COM,i} \tag{H.3}$$

The Euclidean distance between the center of the system and $\mathbf{R}_{COM,i}$ is calculated and if this distance is below some threshold value then we initialise the surface hopping trajectory on that adiabatic state. If we do not find any states within 3KT of the ground state and within an acceptable radius of the center we start again this time increasing the maximum allowed distance from the center. If this maximum allowed distance is increased such that we reach another threshold distance the energy threshold is increased this time until a state is found that is close enough to the center. In this way we find an adiabatic state, which when transformed, gives a diabatic population close to center of the system and near the ground state energy.

Appendix I

Analytic Overlap Method

Appendix J

Colophon

This is a description of the tools you used to make your thesis. It helps people make future documents, reminds you, and looks good.

(example) This document was set in the Times Roman typeface using LaTeX(specifically LuaTeX) and BibTeX, composed with Vim Used Archer, Kathleen etc...

Bibliography

[1] Federica Agostini, Ali Abedi, Yasumitsu Suzuki, Seung Kyu Min, Neepa T. Maitra, and E. K. U. Gross. The exact forces on classical nuclei in non-adiabatic charge transfer. The Journal of Chemical Physics, 142(8):084303, February 2015.

[2] Federica Agostini, Seung Kyu Min, Ali Abedi, and E. K. U. Gross. Quantum-Classical Nonadiabatic Dynamics: Coupled- vs Independent-Trajectory Methods. Journal of Chemical Theory and Computation, 12(5):2127–2143, May 2016.

[3] Graeme H. Gossel, Federica Agostini, and Neepa T. Maitra. Coupled-Trajectory Mixed Quantum-Classical Algorithm: A Deconstruction. Journal of Chemical Theory and Computation, August 2018.

[4] William Humphrey, Andrew Dalke, and Klaus Schulten. VMD – Visual Molecular Dynamics. Journal of Molecular Graphics, 14:33–38, 1996.

[5] John Stone. An Efficient Library for Parallel Ray Tracing and Animation. Master's thesis, Computer Science Department, University of Missouri-Rolla, April 1998.

[6] C. K. Chiang, C. R. Fincher, Y. W. Park, A. J. Heeger, H. Shirakawa, E. J. Louis, S. C. Gau, and Alan G. MacDiarmid. Electrical Conductivity in Doped Polyacetylene. Physical Review Letters, 39(17):1098–1101, October 1977.

[7] Hideki Shirakawa, Edwin J. Louis, Alan G. MacDiarmid, Chwan K. Chiang, and Alan J. Heeger. Synthesis of electrically conducting organic polymers: halogen derivatives of polyacetylene, (CH)x. J. Chem. Soc., Chem. Commun., 0(16):578–580, Jan 1977.

[8] Bernard Kippelen and Jean-Luc Brédas. Organic photovoltaics. Energy Environ. Sci., 2(3):251–261, 2009.

[9] M. J. Małachowski and J. Żmija. Organic field-effect transistors. Opto-Electron. Rev., 18(2):121–136, Jun 2010.

[10] N. Thejo Kalyani and S. J. Dhoble. Organic light emitting diodes: Energy saving lighting technology—A review. Renewable Sustainable Energy Rev., 16(5):2696–2723, Jun 2012.

[11] Sebastian Reineke, Frank Lindner, Gregor Schwartz, Nico Seidler, Karsten Walzer, Björn Lüssem, and Karl Leo. White organic light-emitting diodes with fluorescent tube efficiency. Nature, 459(7244):234, May 2009.

[12] Kazuki Kato, Toshihiko Iwasaki, and Takatoshi Tsujimura. Over 130 lm/w all-phosphorescent white oleds for next-generation lighting. Journal of Photopolymer Science and Technology, 28:335–340, 10 2015.

[13] Veaceslav Coropceanu, Jérôme Cornil, Demetrio A. da Silva Filho, Yoann Olivier, Robert Silbey, and Jean-Luc Brédas. Charge Transport in Organic Semiconductors. Chemical Reviews, 107(4):926–952, April 2007.

[14] Samuele Giannini, Antoine Carof, Matthew Ellis, Hui Yang, Orestis George Ziogos, Soumya Ghosh, and Jochen Blumberger. Quantum localization and delocalization of charge carriers in organic semiconducting crystals. Nature Communications, 10(1):3843, Aug 2019.

[15] Alessandro Troisi. Charge transport in high mobility molecular semiconductors: classical models and new theories. Chem. Soc. Rev., 40:2347–2358, 2011.

[16] Simone Fratini, Didier Mayou, and Sergio Ciuchi. The transient localization scenario for charge transport in crystalline organic materials. Advanced Functional Materials, 26(14):2292–2315, 2016.

[17] I. Yavuz. Dichotomy between the band and hopping transport in organic crystals: insights from experiments. Physical Chemistry Chemical Physics, 19(38):25819–25828, 2017.

[18] J. S. Brown and S. E. Shaheen. Introducing correlations into carrier transport simulations of disordered materials through seeded nucleation: impact on density of states, carrier mobility, and carrier statistics. J. Phys.: Condens. Matter, 30(13):135702, Mar 2018.

[19] Tino Zimmerling and Bertram Batlogg. Improving charge injection in high-mobility rubrene crystals: From contact-limited to channel-dominated transistors. Journal of Applied Physics, 115(16):164511, 2014.

[20] V. Podzorov, E. Menard, A. Borissov, V. Kiryukhin, J. A. Rogers, and M. E. Gershenson. Intrinsic charge transport on the surface of organic semiconductors. Phys. Rev. Lett., 93:086602, Aug 2004.

[21] Samuele Giannini, Antoine Carof, and Jochen Blumberger. Crossover from Hopping to Band-Like Charge Transport in an Organic Semiconductor Model: Atomistic Nonadiabatic Molecular Dynamics Simulation. The Journal of Physical Chemistry Letters, 9(11):3116–3123, June 2018.

[22] Harald Oberhofer, Karsten Reuter, and Jochen Blumberger. Charge Transport in Molecular Materials: An Assessment of Computational Methods. Chemical Reviews, 117(15):10319–10357, August 2017.

[23] John C. Tully. Nonadiabatic Dynamics. pages 34–71.

[24] Simone Pisana, Michele Lazzeri, Cinzia Casiraghi, Kostya S. Novoselov, A. K. Geim, Andrea C. Ferrari, and Francesco Mauri. Breakdown of the adiabatic Born–Oppenheimer approximation in graphene. Nat. Mater., 6(3):198, Feb 2007.

[25] M. Born and R. Oppenheimer. Zur Quantentheorie der Molekeln. Ann. Phys., 389(20):457–484, Jan 1927.

[26] Sharon Hammes-Schiffer. Theoretical Perspectives on Proton-Coupled Electron Transfer Reactions. Acc. Chem. Res., 34(4):273–281, Apr 2001.

[27] Sharon Hammes-Schiffer and John C. Tully. Proton transfer in solution: Molecular dynamics with quantum transitions. J. Chem. Phys., 101(6):4657–4667, Sep 1994.

[28] My Hang V. Huynh and Thomas J. Meyer. Proton-coupled electron transfer. Chemical Reviews, 107(11):5004–5064, Nov 2007.

[29] John C. Tully. Nonadiabatic molecular dynamics. International Journal of Quantum Chemistry, 40(S25):299–309, 1991.

[30] Raymond Kapral and Giovanni Ciccotti. Mixed quantum-classical dynamics. J. Chem. Phys., 110(18):8919–8929, May 1999.

[31] Todd J. Martínez∗. Insights for Light-Driven Molecular Devices from Ab Initio Multiple Spawning Excited-State Dynamics of Organic and Biological Chromophores. American Chemical Society, Oct 2005.

[32] Guillermo Albareda, Heiko Appel, Ignacio Franco, Ali Abedi, and Angel Rubio. Correlated Electron-Nuclear Dynamics with Conditional Wave Functions. Phys. Rev. Lett., 113(8):083003, Aug 2014.

[33] John C. Tully. Molecular dynamics with electronic transitions. J. Chem. Phys., 93(2):1061–1071, Jul 1990.

[34] R. L et al Whetten. Molecular dynamics beyond the adiabatic approximation: New experiments and theory. Ann. Rev. Phys. Chem., 36:277–320.

[35] Neil Shenvi, Joseph E. Subotnik, and Weitao Yang. Simultaneous-trajectory surface hopping: A parameter-free algorithm for implementing decoherence in nonadiabatic dynamics. J. Chem. Phys., 134(14):144102, Apr 2011.

[36] D. F. Coker and L. Xiao. Methods for molecular dynamics with nonadiabatic transitions. J. Chem. Phys., 102(1):496–510, Jan 1995.

[37] Joseph E. Subotnik, Amber Jain, Brian Landry, Andrew Petit, Wenjun Ouyang, and Nicole Bellonzi. Understanding the surface hopping view of electronic transitions and decoherence. Annual Review of Physical Chemistry, 67(1):387–417, 2016. PMID: 27215818.

[38] Giovanni Granucci, Maurizio Persico, and Alberto Zoccante. Including quantum decoherence in surface hopping. The Journal of Chemical Physics, 133(13):134111, 2010.

[39] Heather M. Jaeger, Sean Fischer, and Oleg V. Prezhdo. Decoherence-induced surface hopping. The Journal of Chemical Physics, 137(22):22A545, 2012.

[40] Amber Jain, Ethan Alguire, and Joseph E. Subotnik. An efficient, augmented surface hopping algorithm that includes decoherence for use in large-scale simulations. Journal of Chemical Theory and Computation, 12(11):5256–5268, Nov 2016.

[41] Joseph E. Subotnik and Neil Shenvi. A new approach to decoherence and momentum rescaling in the surface hopping algorithm. The Journal of Chemical Physics, 134(2):024105, 2011.

[42] Xiaosong Li, John C. Tully, H. Bernhard Schlegel, and Michael J. Frisch. Ab initio Ehrenfest dynamics. J. Chem. Phys., 123(8):084106, Aug 2005.

[43] Kenichiro Saita and Dmitrii V. Shalashilin. On-the-fly ab initio molecular dynamics with multiconfigurational Ehrenfest method. J. Chem. Phys., 137(22):22A506, Dec 2012.

[44] Daniela Kohen, Frank H. Stillinger, and John C. Tully. Model studies of nonadiabatic dynamics. J. Chem. Phys., 109(12):4713–4725, Sep 1998.

[45] John C. Tully. Perspective: Nonadiabatic dynamics theory. The Journal of Chemical Physics, 137(22):22A301, December 2012.

[46] Priya V. Parandekar and John C. Tully. Detailed Balance in Ehrenfest Mixed Quantum-Classical Dynamics. Journal of Chemical Theory and Computation, 2(2):229–235, March 2006.

[47] Ali Abedi, Neepa T. Maitra, and E. K. U. Gross. Exact Factorization of the Time-Dependent Electron-Nuclear Wave Function. Physical Review Letters, 105(12), September 2010.

[48] Federica Agostini, Seung Kyu Min, and E. K. U. Gross. Semiclassical analysis of the electron-nuclear coupling in electronic non-adiabatic processes. Annalen der Physik, 527(9-10):546–555, October 2015.

[49] Federica Agostini, Ali Abedi, Yasumitsu Suzuki, and E.K.U. Gross. Mixed quantum-classical dynamics on the exact time-dependent potential energy surface: a fresh look at non-adiabatic processes. Molecular Physics, 111(22-23):3625–3640, December 2013.

[50] Ali Abedi, Federica Agostini, Yasumitsu Suzuki, and E. K. U. Gross. Dynamical Steps that Bridge Piecewise Adiabatic Shapes in the Exact Time-Dependent Potential Energy Surface. Physical Review Letters, 110(26), June 2013.

[51] Seung Kyu Min, Ali Abedi, Kwang S. Kim, and E. K. U. Gross. Is the Molecular Berry Phase an Artifact of the Born-Oppenheimer Approximation? Phys. Rev. Lett., 113(26):263004, Dec 2014.

[52] Farnaz A. Shakib and Pengfei Huo. Ring Polymer Surface Hopping: Incorporating Nuclear Quantum Effects into Nonadiabatic Molecular Dynamics Simulations. J. Phys. Chem. Lett., 8(13):3073–3080, Jul 2017.

[53] Basile F. E. Curchod, Ivano Tavernelli, and Ursula Rothlisberger. Trajectory-based solution of the nonadiabatic quantum dynamics equations: an on-the-fly approach for molecular dynamics simulations. PCCP, 13(8):3231–3236, Feb 2011.

[54] Ivano Tavernelli. Ab initio–driven trajectory-based nuclear quantum dynamics in phase space. Phys. Rev. A, 87(4):042501, Apr 2013.

[55] Arne Scherrer, Federica Agostini, Daniel Sebastiani, E. K. U. Gross, and Rodolphe Vuilleumier. Nuclear velocity perturbation theory for vibrational circular dichroism:

An approach based on the exact factorization of the electron-nuclear wave function. J. Chem. Phys., 143(7):074106, Aug 2015.

[56] Seung Kyu Min, Federica Agostini, Ivano Tavernelli, and E. K. U. Gross. Ab Initio Nonadiabatic Dynamics with Coupled Trajectories: A Rigorous Approach to Quantum (De)Coherence. The Journal of Physical Chemistry Letters, 8(13):3048–3055, July 2017.

[57] John C. Tully. Molecular dynamics with electronic transitions. The Journal of Chemical Physics, 93(2):1061–1071, July 1990.

[58] Fruzsina Gajdos, Siim Valner, Felix Hoffmann, Jacob Spencer, Marian Breuer, Adam Kubas, Michel Dupuis, and Jochen Blumberger. Ultrafast Estimation of Electronic Couplings for Electron Transfer between -Conjugated Organic Molecules. Journal of Chemical Theory and Computation, 10(10):4653–4660, October 2014.

[59] J. VandeVondele, J; Hutter. Gaussian basis sets for accurate calculations on molecular systems in gas and condensed phases. The Journal of Chemical Physics, 127(11).

[60] J. Spencer, F. Gajdos, and J. Blumberger. FOB-SH: Fragment orbital-based surface hopping for charge carrier transport in organic and biological molecules and materials. The Journal of Chemical Physics, 145(6):064102, August 2016.

[61] Steven L. Fiedler and Jussi Eloranta. Nonadiabatic dynamics by mean-field and surface-hopping approaches: energy conservation considerations. Molecular Physics, 108(11):1471–1479, 2010.

[62] Joseph E. Subotnik. Augmented ehrenfest dynamics yields a rate for surface hopping. The Journal of Chemical Physics, 132(13):134112, 2010.

[63] K.E. Atkinson. An Introduction to Numerical Analysis. Wiley, 1989.

[64] R.B. Leighton Richard P. Feynman. The Feynman Lectures on Physics, Vol 3. Addison–Wesley, 1998.

[65] James Kirkpatrick. An approximate method for calculating transfer integrals based on the zindo hamiltonian. International Journal of Quantum Chemistry, 108(1):51–56, 2008.

[66] Harald Oberhofer and Jochen Blumberger. Revisiting electronic couplings and incoherent hopping models for electron transport in crystalline c60 at ambient temperatures. Phys. Chem. Chem. Phys., 14:13846–13852, 2012.

[67] Alessandro Troisi and Giorgio Orlandi. Hole migration in dna: a theoretical analysis of the role of structural fluctuations. The Journal of Physical Chemistry B, 106(8):2093–2101, Feb 2002.

[68] Adam Kubas, Felix Hoffmann, Alexander Heck, Harald Oberhofer, Marcus Elstner, and Jochen Blumberger. Electronic couplings for molecular charge transfer: Benchmarking cdft, fodft, and fodftb against high-level ab initio calculations. The Journal of Chemical Physics, 140(10):104105, 2014.

[69] Adam Kubas, Fruzsina Gajdos, Alexander Heck, Harald Oberhofer, Marcus Elstner, and Jochen Blumberger. Electronic couplings for molecular charge transfer: benchmarking cdft, fodft and fodftb against high-level ab initio calculations. ii. Phys. Chem. Chem. Phys., 17:14342–14354, 2015.

[70] Antoine Carof, Samuele Giannini, and Jochen Blumberger. Detailed balance, internal consistency, and energy conservation in fragment orbital-based surface hopping. The Journal of Chemical Physics, 147(21):214113, December 2017.

[71] Antoine Carof, Samuele Giannini, and Jochen Blumberger. Detailed balance, internal consistency, and energy conservation in fragment orbital-based surface hopping. The Journal of Chemical Physics, 147(21):214113, 2017.

[72] Soumya Ghosh, Samuele Giannini, Kevin Lively, and Jochen Blumberger. Nonadiabatic dynamics with quantum nuclei: simulating charge transfer with ring polymer surface hopping. Faraday Discuss., 221:501–525, 2020.

[73] Antoine Carof, Samuele Giannini, and Jochen Blumberger. How to calculate charge mobility in molecular materials from surface hopping non-adiabatic molecular dynamics – beyond the hopping/band paradigm. Phys. Chem. Chem. Phys., 21:26368–26386, 2019.

[74] J. Spencer, F. Gajdos, and J. Blumberger. Fob-sh: Fragment orbital-based surface hopping for charge carrier transport in organic and biological molecules and materials. The Journal of Chemical Physics, 145(6):064102, 2016.

[75] Jacob Spencer, Laura Scalfi, Antoine Carof, and Jochen Blumberger. Confronting surface hopping molecular dynamics with marcus theory for a molecular donor–acceptor system. Faraday Discuss., 195:215–236, 2016.

[76] Samuele Giannini, Orestis George Ziogos, Antoine Carof, Matthew Ellis, and Jochen Blumberger. Flickering polarons extending over ten nanometres mediate charge transport in high-mobility organic crystals. Advanced Theory and Simulations, 3(9):2000093, 2020.

[77] Samuele Giannini, Antoine Carof, and Jochen Blumberger. Crossover from hopping to band-like charge transport in an organic semiconductor model: Atomistic nonadiabatic molecular dynamics simulation. The Journal of Physical Chemistry Letters, 9(11):3116–3123, Jun 2018.

[78] Orestis George Ziogos, Samuele Giannini, Matthew Ellis, and Jochen Blumberger. Identifying high-mobility tetracene derivatives using a non-adiabatic molecular dynamics approach. J. Mater. Chem. C, 8:1054–1064, 2020.

[79] Fruzsina Gajdos, Siim Valner, Felix Hoffmann, Jacob Spencer, Marian Breuer, Adam Kubas, Michel Dupuis, and Jochen Blumberger. Ultrafast estimation of electronic couplings for electron transfer between π-conjugated organic molecules. Journal of Chemical Theory and Computation, 10(10):4653–4660, Oct 2014.

[80] Biswajit Ray, Aditya G. Baradwaj, Bryan W. Boudouris, and Muhammad A. Alam. Defect characterization in organic semiconductors by forward bias capacitance–

voltage (fb-cv) analysis. The Journal of Physical Chemistry C, 118(31):17461–17466, Aug 2014.

[81] W. S. Hu, Y. T. Tao, Y. J. Hsu, D. H. Wei, and Y. S. Wu. Molecular orientation of evaporated pentacene films on gold: alignment effect of self-assembled monolayer. Langmuir, 21(6):2260–2266, Mar 2005.

[82] Tatsuo Hasegawa and Jun Takeya. Organic field-effect transistors using single crystals. Science and Technology of Advanced Materials, 10(2):024314, 2009.

[83] John E. Anthony, James S. Brooks, David L. Eaton, and Sean R. Parkin. Functionalized pentacene: improved electronic properties from control of solid-state order. Journal of the American Chemical Society, 123(38):9482–9483, Sep 2001.

[84] John E. Anthony, David L. Eaton, and Sean R. Parkin. A road map to stable, soluble, easily crystallized pentacene derivatives. Organic Letters, 4(1):15–18, Jan 2002.

[85] A. D'Angelo, B. Edgar, A. P. Hurt, and M. D. Antonijević. Physico-chemical characterisation of three-component co-amorphous systems generated by a melt-quench method. Journal of Thermal Analysis and Calorimetry, 134(1):381–390, Oct 2018.

[86] Wanderlã L. Scopel, Antônio J. R. da Silva, and A. Fazzio. Amorphous hfo_2 and $hf_{1-x}si_xO$ via a melt-and-quench scheme using ab initio molecular dynamics. Phys. Rev. B, 77:172101, May 2008.

[87] Seth S. Berbano, Inseok Seo, Christian M. Bischoff, Katherine E. Schuller, and Steve W. Martin. Formation and structure of na2s+p2s5 amorphous materials prepared by melt-quenching and mechanical milling. Journal of Non-Crystalline Solids, 358(1):93 – 98, 2012.

[88] Pranav Karmwar, Kirsten Graeser, Keith C. Gordon, Clare J. Strachan, and Thomas Rades. Investigation of properties and recrystallisation behaviour of amorphous indomethacin samples prepared by different methods. International Journal of Pharmaceutics, 417(1):94 – 100, 2011. Advanced characterization techniques.

[89] Min-Jin Ko, Joel Plawsky, and Meyer Birnboim. Fabrication of cds/ag hybrid quantum dot composites using a melt/quench method. Journal of Non-Crystalline Solids, 203:211 – 216, 1996. Optical and Electrical Propertias of Glasses.

[90] Steve Plimpton. Fast parallel algorithms for short-range molecular dynamics. Journal of Computational Physics, 117(1):1 – 19, 1995.

[91] Steve Plimpton. Lammps software. http://lammps.sandia.gov, 1995. [Online; accessed 21-Jan-2021].

[92] Steve Plimpton, Roy Pollock, and Mark Stevens. Particle-mesh ewald and rrespa for parallel molecular dynamics simulations. In In Proceedings of the Eighth SIAM Conference on Parallel Processing for Scientific Computing, 1997.

[93] Christopher I. Bayly, Piotr Cieplak, C, and Peter A. Kollman. A well-behaved electrostatic potential based method using charge restraints for deriving atomic charges: the resp model. The Journal of Physical Chemistry, 97(40):10269–10280, Oct 1993.

[94] M. J. Frisch, G. W. Trucks, H. B. Schlegel, G. E. Scuseria, M. A. Robb, J. R. Cheeseman, G. Scalmani, V. Barone, G. A. Petersson, H. Nakatsuji, X. Li, M. Caricato, A. V. Marenich, J. Bloino, B. G. Janesko, R. Gomperts, B. Mennucci, H. P. Hratchian, J. V. Ortiz, A. F. Izmaylov, J. L. Sonnenberg, D. Williams-Young, F. Ding, F. Lipparini, F. Egidi, J. Goings, B. Peng, A. Petrone, T. Henderson, D. Ranasinghe, V. G. Zakrzewski, J. Gao, N. Rega, G. Zheng, W. Liang, M. Hada, M. Ehara, K. Toyota, R. Fukuda, J. Hasegawa, M. Ishida, T. Nakajima, Y. Honda, O. Kitao, H. Nakai, T. Vreven, K. Throssell, J. A. Montgomery, Jr., J. E. Peralta, F. Ogliaro, M. J. Bearpark, J. J. Heyd, E. N. Brothers, K. N. Kudin, V. N. Staroverov, T. A. Keith, R. Kobayashi, J. Normand, K. Raghavachari, A. P. Rendell, J. C. Burant, S. S. Iyengar, J. Tomasi, M. Cossi, J. M. Millam, M. Klene, C. Adamo, R. Cammi, J. W. Ochterski, R. L. Martin, K. Morokuma, O. Farkas, J. B. Foresman, and D. J. Fox. Gaussian˜16 Revision C.01, 2016. Gaussian Inc. Wallingford CT.

[95] Junmei Wang, Romain M. Wolf, James W. Caldwell, Peter A. Kollman, and David A. Case. Development and testing of a general amber force field. Journal of Computational Chemistry, 25(9):1157–1174, 2004.

[96] Makoto Yoneya, Masahiro Kawasaki, and Masahiko Ando. Molecular dynamics simulations of pentacene thin films: The effect of surface on polymorph selection. J. Mater. Chem., 20:10397–10402, 2010.

[97] Makoto Yoneya, Masahiro Kawasaki, and Masahiko Ando. Are pentacene monolayer and thin-film polymorphs really substrate-induced? a molecular dynamics simulation study. The Journal of Physical Chemistry C, 116(1):791–795, Jan 2012.

[98] Makoto Yoneya. Simulation of crystallization of pentacene and its derivatives from solution. The Journal of Physical Chemistry C, Jan 2021.

[99] Ryan A. Miller, Amanda Larson, and Karsten Pohl. Novel surface diffusion characteristics for a robust pentacene derivative on au(111) surfaces. Chemical Physics Letters, 678:28 – 34, 2017.

[100] Dong Wang, Ling Tang, Mengqiu Long, and Zhigang Shuai. Anisotropic thermal transport in organic molecular crystals from nonequilibrium molecular dynamics simulations. The Journal of Physical Chemistry C, 115(13):5940–5946, Apr 2011.

[101] Florian Steiner, Carl Poelking, Dorota Niedzialek, Denis Andrienko, and Jenny Nelson. Influence of orientation mismatch on charge transport across grain boundaries in tri-isopropylsilylethynyl (tips) pentacene thin films. Phys. Chem. Chem. Phys., 19:10854–10862, 2017.

[102] Ida Bagus Hendra Prastiawan, Jingxiang Xu, Yusuke Ootani, Yuji Higuchi, Nobuki Ozawa, Shingo Maruyama, Yuji Matsumoto, and Momoji Kubo. Molecular interactions between pentacene and imidazolium ionic liquids: A molecular dynamics study. Chemistry Letters, 47(9):1154–1157, 2018.

[103] EPA DSSTox. Epa dsstox. https://comptox.epa.gov/dashboard/DTXSID7059648, 2021. [Online; accessed 25-Jan-2021].

[104] Stefan Schiefer, Martin Huth, Alexander Dobrinevski, and Bert Nickel. Determination of the crystal structure of substrate-induced pentacene polymorphs in fiber structured thin films. Journal of the American Chemical Society, 129(34):10316–10317, Aug 2007.

[105] Martin Ester, Hans-Peter Kriegel, Jörg Sander, and Xiaowei Xu. A density-based algorithm for discovering clusters in large spatial databases with noise. pages 226–231. AAAI Press, 1996.

[106] John C. Tully. Molecular dynamics with electronic transitions. The Journal of Chemical Physics, 93(2):1061–1071, 1990.

[107] P. P. Ewald. Die berechnung optischer und elektrostatischer gitterpotentiale. Annalen der Physik, 369(3):253–287, 1921.

[108] D. Wolf, P. Keblinski, S. R. Phillpot, and J. Eggebrecht. Exact method for the simulation of coulombic systems by spherically truncated, pairwise r−1 summation. The Journal of Chemical Physics, 110(17):8254–8282, 1999.

[109] Dirk Zahn, Bernd Schilling, and Stefan M. Kast. Enhancement of the wolf damped coulomb potential: static, dynamic, and dielectric properties of liquid water from molecular simulation. The Journal of Physical Chemistry B, 106(41):10725–10732, Oct 2002.

[110] Christopher J. Fennell and J. Daniel Gezelter. Is the ewald summation still necessary? pairwise alternatives to the accepted standard for long-range electrostatics. The Journal of Chemical Physics, 124(23):234104, 2006.

[111] Colin R. Groom, Ian J. Bruno, Matthew P. Lightfoot, and Suzanna C. Ward. The Cambridge Structural Database. Acta Crystallographica Section B, 72(2):171–179, Apr 2016.